Fracture and fatigue of ideal polymer networks

Shaoting Lin [a], Jiahua Ni [a], Dongchang Zheng [a], Xuanhe Zhao [a,b,*]

[a] *Department of Mechanical Engineering, Massachusetts Institute of Technology, Cambridge, MA, USA*
[b] *Department of Civil and Environmental Engineering, Massachusetts Institute of Technology, Cambridge, MA, USA*

ARTICLE INFO

ABSTRACT

Soft materials have enabled diverse modern technologies, but their practical deployment is usually limited by their mechanical failures. Fracture and fatigue of polymer networks are two important causes of mechanical failures of soft materials. A soft material fails by fracture when a monotonic load reaches its fracture toughness or fails by fatigue when a cyclic load reaches its fatigue threshold. The fracture toughness is usually much higher than the fatigue threshold for randomly crosslinked elastomers and gels. While fracture and fatigue have been extensively studied in randomly crosslinked elastomers and gels, they have not been comparatively studied in polymer networks with well-controlled architectures and defects. This work systematically studies the fracture and fatigue of ideal polymer networks with controlled densities of dangling-chain defects. We show that the fracture toughness and fatigue threshold of an ideal polymer network almost without defects are the same. After introducing a low density of dangling-chain defects into the ideal polymer network, its fracture toughness and fatigue threshold still maintain approximately the same. The fracture toughness of the ideal polymer network is also independent of the loading rate. We further use the recently developed defect-network model to explain the fatigue threshold (*i.e.*, intrinsic fracture energy) of ideal polymer networks with controlled densities of dangling-chain defects.

© 2021 Elsevier Ltd. All rights reserved.

1. Introduction

Soft materials including elastomers and gels have enabled a variety of modern technologies with examples as diverse as soft robots [1–3], bioelectronics [4–7], tissue adhesives [8,9], biosensing [10–12], and water harvesters [13–15]. However, the practical deployment of these technologies is usually limited by the mechanical failures of soft materials. For example, a crack can propagate in a piece of a soft material when a monotonic mechanical load on the material reaches a critical value, causing the fracture failure [16,17]. As another example, the crack can also propagate in the material when a cyclic load on the material reaches another critical value, leading to the fatigue failure [18,19]. Fracture and fatigue of polymer networks represent two important causes of mechanical failures of soft materials. Designing high toughness and high fatigue resistance for soft materials is crucial for their robustness and functions in modern technologies.

Over the last few decades, burgeoning experimental efforts have been made to understand fracture and fatigue of soft materials using randomly crosslinked polymer networks, which contain non-uniform chain length (*i.e.*, the number of monomers in a chain connected by neighboring cross-links), non-uniform

functionality (*i.e.*, the number of chains connected to one cross-link), chain entanglements, and/or uncontrolled topological defects (*e.g.*, dangling chains, cyclic loops) [20–22]. For example, Yang et al. studied the effect of network imperfection on the fracture toughness of polyacrylamide hydrogels [23]. They attributed the unexpected high toughness of polyacrylamide hydrogels to the non-uniform chain lengths and distributed chain scissions around the crack. Slootman et al. used mechanochemistry to characterize the spatial distribution of bond scission around crack surfaces in elastomers [24]. They reported that the bond scissions near the crack plane are rate-dependent and can be delocalized over up to hundreds of micrometers. Similarly, Matsuda et al. used mechano-radical polymerization of thermo-responsive fluorescent polymers to visualize the chain scission around the crack tip of double-network hydrogels [25]. While fracture and fatigue have been extensively studied in these randomly crosslinked elastomers and gels, they have not been comparatively studied in polymer networks with well-controlled architectures and defects. Such well-controlled polymer networks can potentially provide better understanding on mechanical failures of polymer networks by directly connecting experimental results to theoretical models [26].

Here, we systematically study the fracture and fatigue of ideal polymer networks with nearly uniform chain length and functionality, no entanglement, and controlled densities of dangling-chain defects (Fig. 1a). Our experimental results show that the

---

* Corresponding author.
E-mail address: zhaox@mit.edu (X. Zhao).
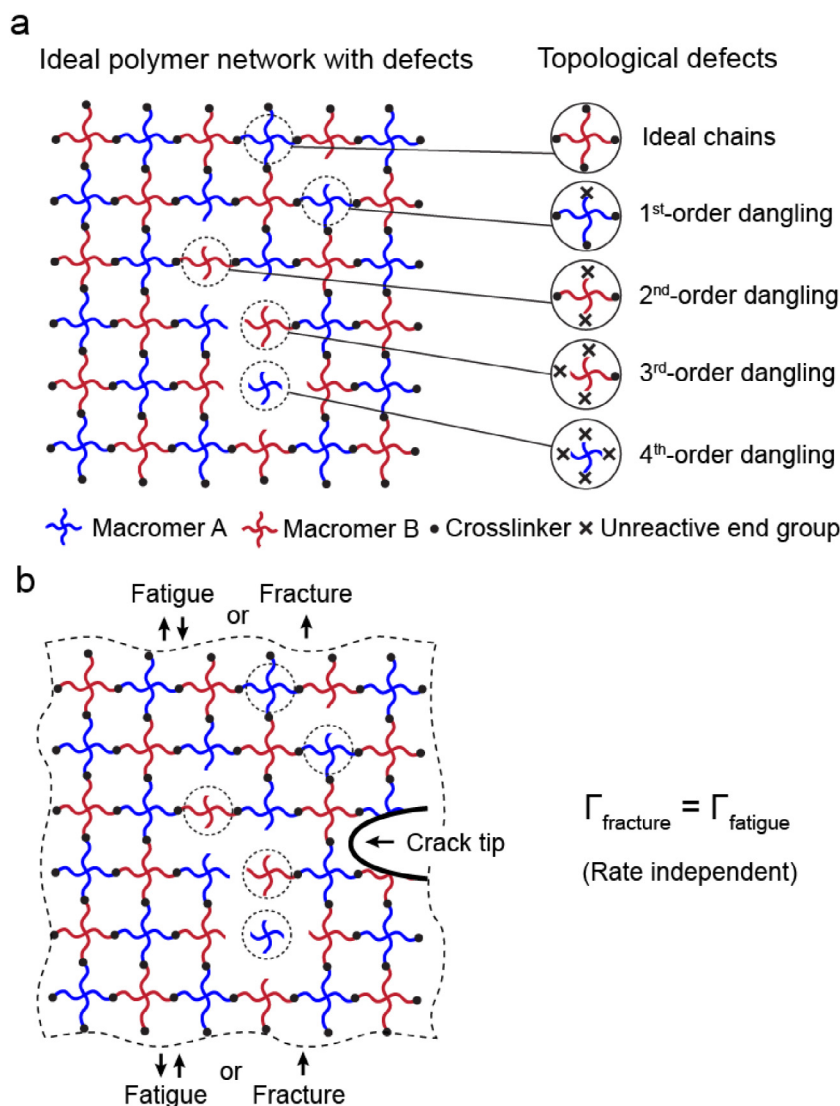
Fig. 1. Fracture and fatigue of ideal polymer networks. (a) Schematic illustration of ideal polymer networks containing various topological defects such as dangling chains. (b) Fracture toughness and fatigue threshold of ideal polymer networks without defects and with low-density defects are the same (*i.e.*, $\Gamma_{\text{fracture}} = \Gamma_{\text{fatigue}}$), which are also independent of the loading rate.

fracture toughness Γ_{fracture} and fatigue threshold Γ_{fatigue} of an ideal polymer network almost without defects are the same (*i.e.*, $\Gamma_{\text{fracture}} = \Gamma_{\text{fatigue}}$). After introducing low-density dangling-chain defects into the ideal polymer network, its fracture toughness and fatigue threshold still maintain approximately the same (Fig. 1b). In addition, we show that the measured fracture toughness of an ideal polymer network without defects or with dangling-chain defects is independent of the loading rate (Fig. 1b). We further use the recently developed defect-network model [26] to theoretically explain the fatigue threshold of ideal polymer networks with controlled densities of dangling-chain defects.

The outline of this paper is as follows. In Section 2, we provide the experimental details including fabrication of ideal polymer networks, control of topological defects, and characterization of fracture and fatigue of ideal polymer networks with various dangling-chain defects. In Section 3, we compare the fracture toughness and fatigue threshold of ideal polymer networks, and investigate the rate dependence of fracture toughness of ideal polymer networks. We conclude the current study in Section 4, where we also provide future research directions.

2. Experiments

2.1. Fabrication of ideal polymer networks

We start with the A–B type tetra-arm polyethylene glycol (PEG) hydrogel to prepare ideal polymer networks with a controlled introduction of defects. The A–B type tetra-arm PEG hydrogel contains tetra-amine-terminated PEG macromers (*i.e.*, PEG-NH$_2$, Laysan Bio) and tetra-NHS-terminated PEG macromers (*i.e.*, PEG-NHS, Laysan Bio) (Fig. 2a). The molecular weights of both macromers are 20,000 g/mol with each arm of 5000 g/mol. The synthesis of the tetra-arm PEG hydrogel follows the reported protocol [27]. 100 mg PEG-NH$_2$ is first dissolved and vigorously mixed in 1 mL phosphate buffer solution with a pH of 7.4 and ionic strength of 100 mM. Thereafter, 100 mg PEG-NHS is dissolved and vigorously mixed in 1 mL phosphate-citric acid buffer solution with a pH of 5.8 and ionic strength of 100 mM. To introduce defects by tuning the reaction efficiency p, we incubate the PEG-NHS for a controlled degradation time t_{deg}, during which the NHS group turns to be inactive by hydrolyzing the activated esters (Fig. 2b). Thereafter, both the solutions of PEG-NH$_2$ and PEG-NHS are vigorously mixed and poured
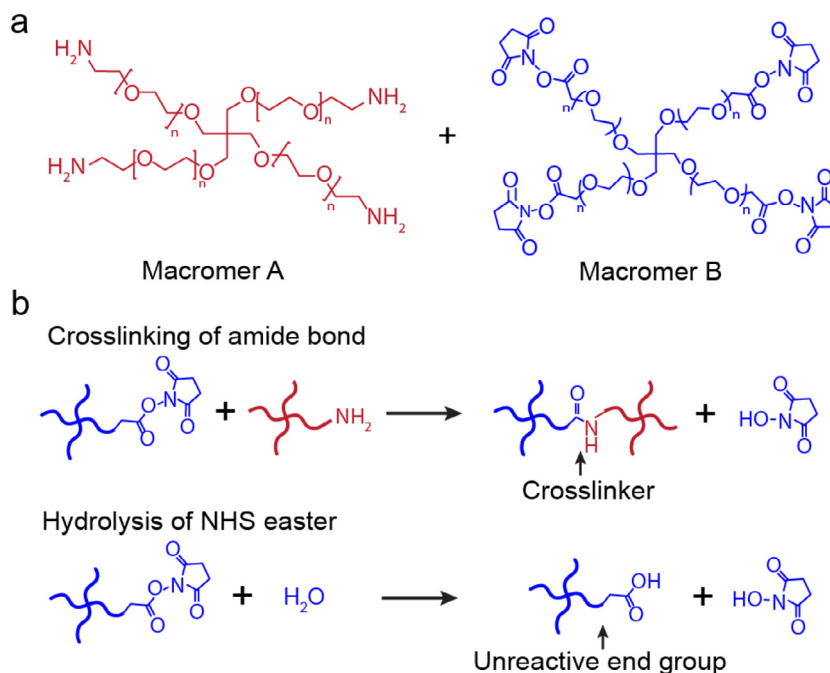
Fig. 2. Chemical structure and chemical reaction of A–B type tetra-arm PEG hydrogels. (a) Chemical structure of PEG-NH$_2$ macromer and PEG-NHS macromer. (b) The NHS ester reacts with the amine group to yield a stable amide bond as the chemical cross-link. The hydrolysis of NHS ester yields an unreactive end group of PEG-NHS macromers.

into a rectangular-shaped mold with the dimensions of 40 mm, 20 mm, and 1.5 mm, giving a final concentration of PEG-NH$_2$ and PEG-NHS macromers as 50 mg/mL, respectively. The final concentrations of PEG-NH$_2$ and PEG-NHS macromers are nearly at the overlap concentration of PEG macromers with a molecular weight of 20,000 g/mol [28], giving negligible inter-/intra- chain interactions. The resultant samples are placed in a humidity chamber for at least 12 h to complete the reaction of forming amide bonds between macromers (Fig. 2b). The samples are further submerged in deionization water to reach their equilibrium swollen states. At least 24 h are required to ensure that the samples reach their fully swollen states.

2.2. Control of topological defects in ideal polymer networks

Since the end groups of the type A PEG macromer and the type B PEG macromer do not have self-reactions and must connect alternatively, the tetra-arm A–B PEG hydrogel has its unique feature of forming near-ideal polymer networks with approximately mono-dispersity, uniform functionality, and negligible defects [29,30]. Such near-ideal polymer network architecture was supported through small-angle neutron scattering [28], dynamic light scattering [29], neutron spin echo spectroscopy [31]. In addition, Fourier-transform infrared spectroscopy was also performed to characterize the number of unreacted groups (or dangling chains) in the tetra-arm PEG hydrogels [32]. The maximum reaction efficiency of the PEG hydrogel was identified as high as 0.93, suggesting negligible unreacted groups in the material.

While the tetra-arm A–B type PEG hydrogel represents a near-ideal polymer network, it still contains two types of defects: dangling chains and cyclic loops [33]. We first estimate the fraction of cyclic loops in our material system based on the reported simulation results [34]. For an ideal network with 100 mg/mL PEG macromers with a molecular weight of 20,000 g/mol, the calculated fraction of secondary loops is approximately 6% per macromer. The fractions of higher-order loops are even lower. For

example, the calculated fractions of fourth-order loops and sixth-order loops are only about 0.2% per macromer. Given the low fractions of various orders of cyclic loops, we can regard the tetra-arm PEG hydrogel as an ideal polymer network containing only dangling-chain defects. The number of dangling chains in a defective macromer defines the order of the defect. For example, the defective macromer containing X dangling chains is defined as the Xth-order dangling-chain defect. In a tetra-arm ideal polymer network, there are four types of dangling-chain defects: 1st-order, 2nd-order, 3rd-order, and 4th-order dangling-chain defects.

The number of each type of dangling-chain defects can be controlled by tuning the reaction efficiency p to form cross-links between PEG-NH$_2$ macromers and PEG-NHS macromers. To tune the reaction efficiency p, we incubate PEG-NHS macromers for a controlled time t_{deg}, during which the activated esters in the NHS groups are hydrolyzed, making the NHS groups inactive and decreasing the reaction efficiency p. To identify the relationship between the reaction efficiency p and the controlled time for incubation t_{deg}, we take the linear form [27] and identify the reduction rate of the reaction efficiency p by fitting the measured modulus of the resultant polymer network with the theoretical model (Fig. 6c and Appendix B.). Fig. 6a plots the identified reaction efficiency p as a function of the controlled incubation time t_{deg}.

2.3. Fracture of ideal polymer networks

We first perform fracture tests of ideal polymer networks with various densities of dangling-chain defects. We use pure shear tensile tests to first measure the nominal stress versus stretch curve (i.e., S vs. λ) of a sample with no crack [16]. We further use a razor blade to introduce a sharp crack in the other sample with the same dimensions as the unnotched sample. We measure the critical stretch (i.e., λ_c), at which crack propagates. The measured fracture toughness can be calculated through $\Gamma_{fracture} = H \int_1^{\lambda_c} S d\lambda$, where H is the height of the sample (Fig. 3a). As plotted in Fig. 3b, the critical stretch increases slightly as the degradation
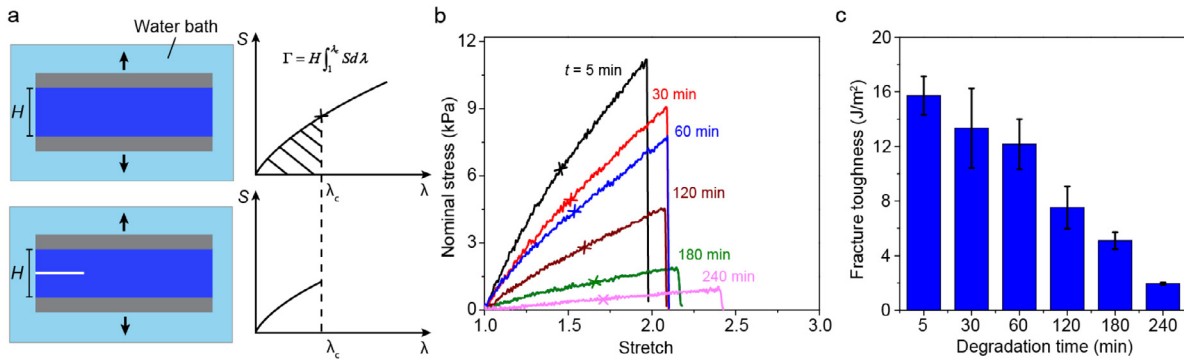
Fig. 3. Fracture test of tetra-arm PEG hydrogels. (a) Schematically illustration of the pure shear tensile test for measuring the fracture toughness. (b) Nominal stress versus stretch curves of tetra-arm PEG hydrogels with various degradation time (5 min, 30 min, 60 min, 120 min, 180 min, 240 min). The cross points indicate the critical point, at which the crack propagates in the corresponding notched sample. (c) Measured fracture toughness as a function of degradation time.

time for NHS groups increases. Accordingly, the measured fracture toughness of ideal polymer networks decreases, manifesting the controlled introduction of dangling-chain defects in the series of samples (Fig. 3c).

2.4. Fatigue of ideal polymer networks

We further perform fatigue fracture tests of ideal polymer networks with various topological defects. As schematically illustrated in Fig. 4a, we cyclically load an unnotched sample to measure the nominal stress versus stretch curve (i.e., S vs. λ) under pure shear tensile loading [35]. Unlike most synthetic hydrogels, the ideal polymer networks show no hysteresis loop and no rate dependency (Fig. 4b). In addition, a negligible decrease in stress is observed over cycles (Fig. 4c). The slight reduction of the stress is possibly attributed to the poroelasticity of the hydrogel sample. No hysteresis loop, no rate dependency, and negligible decrease of the nominal stress indicate that the ideal polymer networks containing dangling-chain defects are purely elastic and free of mechanical dissipations. The strain energy density stored in the sample over cycles can be calculated through $W\left(\lambda_{\text{applied}}\right) = \int_1^{\lambda_{\text{applied}}} S d\lambda$, where λ_{applied} is the maximum applied stretch, S and λ are the nominal stress and stretch of the sample without crack. Similar to the fracture test, we use a razor blade to introduce a sharp crack in the sample. We perform cyclic loading on the notched sample and use a camera to record the crack extension (i.e., c) over cycles (i.e., N). When the applied maximum stretch is low, there is no crack extension under cyclic loading (i.e., $dc/dN = 0$). We gradually increase the stretch by 0.05. At a critical stretch, the sample shows a rapid crack propagation (Fig. 4d). The maximum applied energy release rate is calculated by $G\left(\lambda_{\text{applied}}\right) = H \int_1^{\lambda_{\text{applied}}} S d\lambda$. Fig. 4e summarizes the measured crack extension rate under cyclic loading dc/dN as a function of the applied energy release rate G for an ideal polymer network with a degradation time of 60 min. There exists a maximum stretch (i.e., λ_m), below which the crack extension rate is strictly zero. We take the critical energy release rate at λ_m as the measured fatigue threshold (i.e., $\Gamma_{\text{fatigue}} = G_c = G\left(\lambda_m\right) = H \int_1^{\lambda_m} S d\lambda$). The fatigue threshold of the ideal polymer network with degradation time of 60 min is measured as 11.6 J/m².

3. Results and discussion

3.1. Comparison between fracture toughness and fatigue threshold

The fracture toughness and fatigue threshold have been intensively measured and reported in various soft materials including natural rubbers [36], dielectric elastomers [37], interpenetrating

tough hydrogels [35], double network hydrogels [38], viscoelastic polyampholyte hydrogels [39], and semi-crystalline hydrogels [40–42]. The measured fatigue thresholds of these soft materials are consistently lower than their fracture toughnesses by orders of magnitude. Even for a nearly elastic and low-hysteresis polyacrylamide hydrogel [42,43], the measured fatigue threshold is still much lower than its fracture toughness. To the best of our knowledge, there has been no reported polymer network giving the same fracture toughness and fatigue threshold.

In this work, we systematically compare the fracture toughness and fatigue threshold of ideal networks with various densities of defects. Our measurements show the fracture toughness and fatigue threshold of ideal polymer networks almost without defects (i.e., $t_{\text{deg}} = 5$ min) and with low-density defects (i.e., $t_{\text{deg}} = 30, 60, 120$ min) are approximately the same (i.e., $\Gamma_{\text{fracture}}/\Gamma_{\text{fatigue}} \approx 1$, Fig. 4f). Using the tetra-arm PEG hydrogel with the degradation time of 60 min as one example, its fatigue threshold is measured as 11.6 J/m², which is approximately the same as its fracture toughness (i.e., 12.2 ± 1.8 J/m²). To further verify the approximately same fracture toughness and fatigue threshold, we record the crack extension of a notched sample in fatigue tests. As shown in Fig. 4d, when the applied energy release rate is below its fatigue threshold, there is no detectable crack extension (the resolution of the camera is 20 μm/pixel) or reduction of force under 1000 cycles of loading; however, when the applied energy release rate exceeds its fatigue threshold, the sample fails by rapid crack propagation under a single cycle of loading.

There are two physical reasons to explain the approximately same fracture toughness and fatigue threshold of ideal polymer networks almost without defects and with low-density defects. First, there should be no mechanical dissipations when cyclically deforming the bulk polymer networks (supported by the negligible hysteresis in Fig. 4b), since such dissipations lead to the difference between fracture toughness and fatigue threshold of polymer networks [35]. Second, there should be no delocalized damage of covalent bond scission from the crack plane once the crack extends, which otherwise results in higher fracture toughness than fatigue threshold in randomly crosslinked elastomers and hydrogels.

When we introduce high-density defects into the ideal polymer network (i.e., $t_{\text{deg}} = 180, 240$ min), we find the fracture toughness is slightly higher than the fatigue threshold (Fig. 4f). This may be due to the slight dissipations induced by substantial dangling chains.
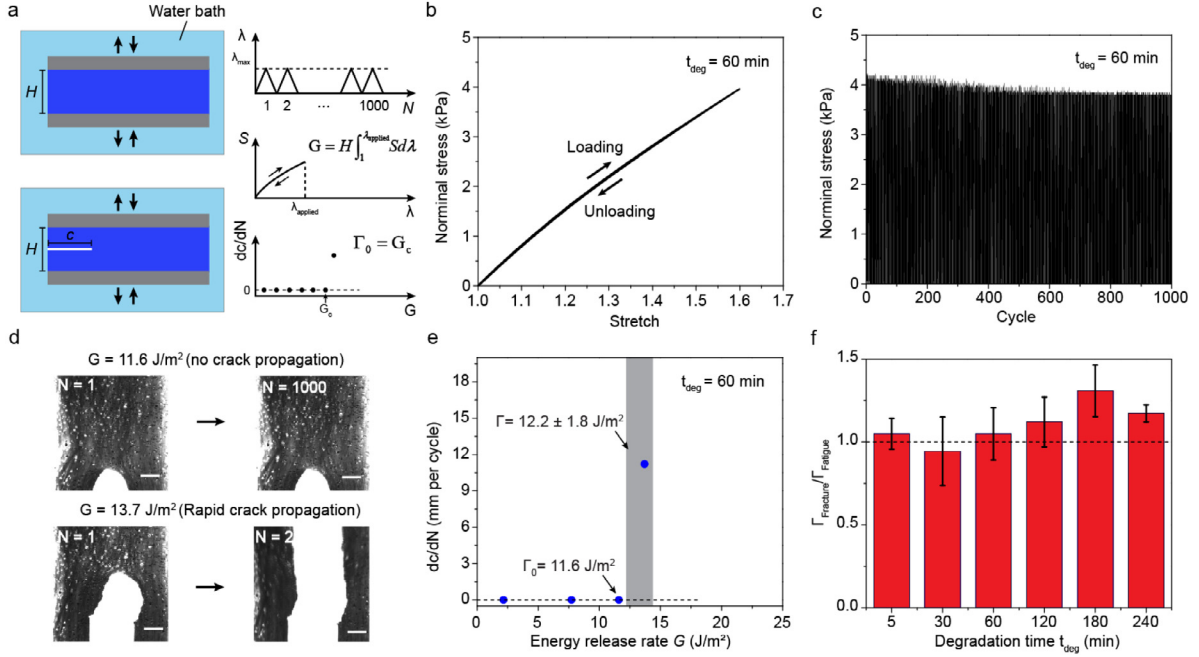
Fig. 4. Fatigue fracture test of tetra-arm PEG hydrogels. (a) Schematically illustration of the pure shear tensile test for measuring the fatigue threshold. (b) Nominal stress versus stretch curves of the tetra-arm PEG hydrogel with the degradation time of 60 min under one cycle of loading. (c) Nominal stress as a function of loading cycle of the tetra-arm PEG hydrogel with the degradation time of 60 min under the maximum loading stretch of 1.6. (d) Images of the notched sample of the tetra-arm PEG hydrogel with the degradation time of 60 min at 1st cycle and 1000th cycle under the maximum applied energy release rate of 11.6 J/m², showing no crack propagation. Images of the same notched sample at 1st cycle and 1000st cycle under the maximum applied energy release rate of 13.7 J/m², showing rapid crack propagation. (e) Fatigue crack extension per cycle dc/dN as a function of the maximum applied energy release rate G, measuring the fatigue threshold of 11.6 J/m². The gray region denotes the domain where the samples fracture under a monotonic loading, measuring the fracture toughness of 12.2 ± 1.8 J/m². (f) Summarized normalized fracture toughness of ideal polymer networks by its fatigue threshold $\Gamma_{fracture}/\Gamma_{fatigue}$ for the tetra-arm PEG hydrogels with various degradation times.

3.2. Rate-independent fracture toughness

The effects of loading rates on fracture toughness of soft materials have been intensively studied in randomly crosslinked polymer networks. Existing studies attribute the rate-dependent fracture toughness to various viscoelastic dissipations such as chain entanglements [44,45] and reversible crosslinks [46–48]. Despite existing studies in randomly crosslinked polymer networks, the effects of loading rates on fracture toughness of ideal polymer networks have not been studied.

Here, we investigate the rate dependence of the ideal polymer networks' fracture toughness. We first measure the nominal stress versus stretch curve of an unnotched PEG hydrogel sample at various loading rates of 0.2, 1, 5, 10, 20 min^{-1}. As shown in Fig. 5a and 5b, there is no rate dependency and negligible hysteresis at various loading rates. We further measure the fracture toughness of ideal polymer networks almost without defects (i.e., $t_{deg} = 5$ min) and with defects (i.e., $t_{deg} = 60$ min). The fracture toughness of ideal polymer networks almost without defects and with defects show no rate dependency either (Fig. 5c–f). This observation suggests the slight introduction of dangling-chain defects in ideal polymer networks does not contribute to the rate dependence of fracture toughness of ideal polymer networks.

3.3. Comparison of experimental results with defect-network model

Let us first consider an ideal polymer network without any defect (i.e., $p = 1$) in the as-prepared reference state. The phantom network model [49,50] and the Lake–Thomas model [20,26,27] predict the shear modulus μ^{ref} and the fatigue threshold (or the intrinsic fracture energy) $\Gamma_{fatigue}^{ref}$ of an ideal polymer network without defect (i.e., $p = 1$) at the as-prepared reference state as

$$\mu^{ref}(p = 1) = \frac{f-2}{f}nkT \tag{1a}$$

$$\Gamma_{fatigue}^{ref}(p = 1) = \alpha n^{2/3}UN \tag{1b}$$

where f is the crosslink functionality, n is the number of active chains per unit volume at the as-prepared reference state, N is the number of monomers per chain, kT is the product of the Boltzmann constant and the absolute temperature, U is the bond energy stored in one monomer at fracture, and $\alpha > 1$ is a dimensionless parameter that accounts for the network architecture's contribution to the fatigue threshold [26].

We next estimate the values of parameters in Eq. (1). The crosslink functionality is identified as $f = 4$ since we use tetra-arm polymer networks. The number of active chains per unit volume at the reference state is equal to $n = 2c_{macromer}M_w^{-1}N_A = 6.02 \times 10^{24}$ m^{-3}, where $c_{macromer} = 100$ mg/mL is the concentration of the overall PEG macromers at the reference state, $M_w = 20,000$ g/mol is the molecular weight of one PEG macromer, and $N_A = 6.02 \times 10^{23}$/mol is the Avogadro constant. The number of PEG monomers in a single chain can be taken as $N = 227$, because the molecular weight of one PEG monomer is 44 g/mol and the molecular weight of one polymer chain is 10,000 g/mol. kT is equal to 4.11×10^{-21}J at room temperature. Because the backbone of one PEG monomer consists of two C–O bonds and one C–C bond, the bond dissociation energy of the PEG monomer is estimated to be three times the lowest covalent bonding energies of C–O bond (356 kJ/mol) or C–C bond (346 kJ/mol) [51], giving the bond dissociation energy of one PEG monomer as 1,038 kJ/mol [27]. Following the historical treatment [27,52], one can take the bond dissociation energy of one PEG monomer as the
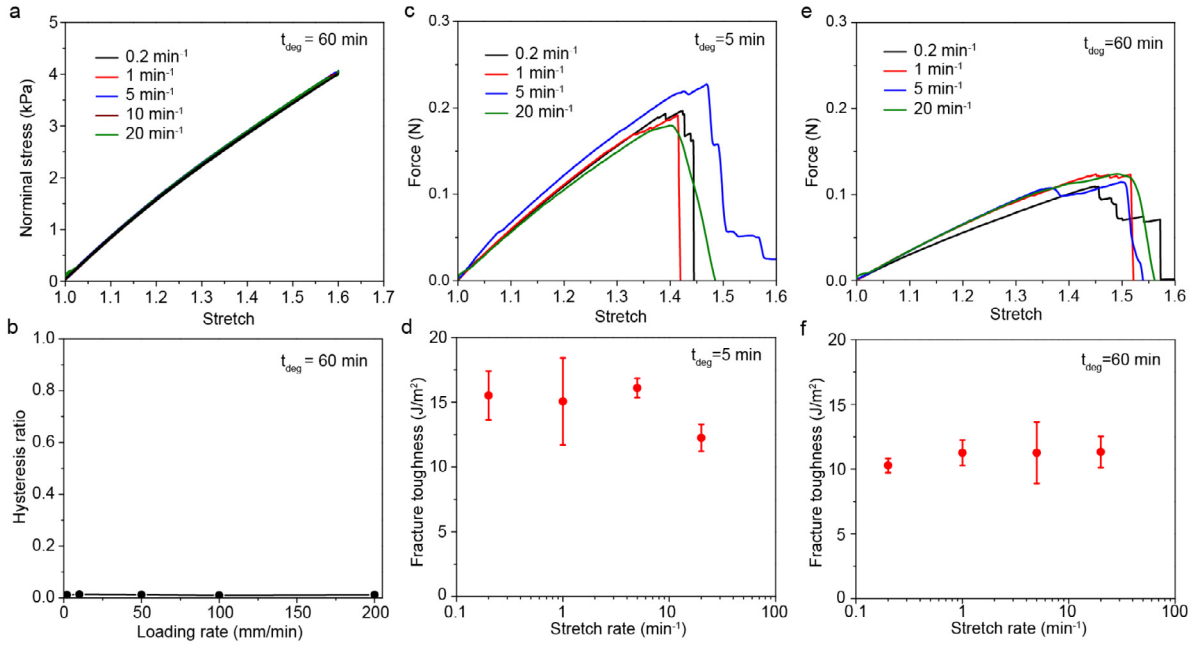
Fig. 5. Fracture toughness of ideal polymer networks at various loading rates. (a) Nominal stress versus stretch curves of an unnotched PEG hydrogel sample with the degradation time of 60 min at the loading rate of 0.2, 1, 5, 10, 20 min^{-1}. (b) Measured hysteresis ratio as a function of various loading rates of the tetra-arm PEG hydrogel with the degradation time of 60 min. (c) Force versus stretch curves of the notched samples and (d) fracture toughness versus stretch rate of the tetra-arm PEG hydrogel with the degradation time of 5 min, representing ideal polymer networks almost without defects. (e) Force versus stretch curves of the notched samples and (f) fracture toughness versus stretch rate of the tetra-arm PEG hydrogel with the degradation time of 60 min, representing ideal polymer networks with defects.

bond energy stored in one monomer at fracture, namely, $U = 1,038$ kJ/mol. Notably, recent studies [53] clarify the difference between the bond energy at fracture and the bond dissociation energy. For example, Wang et al. [53] estimated the bond energy stored in a covalent bond at fracture as 60 kJ/mol, well below the typical values (350–370 kJ/mol) of covalent bond dissociation energies. Mao et al. [54] calculated the bond energy stored in one C–C bond at fracture as 327 kJ/mol through *ab initio* calculations and free energy minimization, slightly lower than its bond dissociation energy (346 kJ/mol). By selecting different U values, one can obtain difference values of α by fitting the theory in Eq. (1b) with experimental results. In this work, we still use $U = 1,038$ kJ/mol for the subsequent calculations. By further substituting the values of N, kT, U, and n, we can identify the shear modulus of an ideal polymer network without defects at the reference state as $\mu^{\mathrm{ref}} (p = 1) = 12.38$ kPa, and the fatigue threshold of an ideal polymer network without defects at the reference state as $\Gamma_{\mathrm{fatigue}}^{\mathrm{ref}} (p = 1) = 12.95\alpha$ J/m^2.

The defect-network model was recently developed to predict the fatigue thresholds [26,55] and shear moduli [26,33,34] of ideal polymer networks with various types of topological defects (see details in Appendix). In particular, for an ideal polymer network with only dangling-chain defects, the dependence of the shear modulus and fatigue threshold at the as-prepared reference state on the reaction efficiency p can be expressed as,

$$\frac{\mu^{\mathrm{ref}} (p)}{\mu^{\mathrm{ref}} (p = 1)} = 1 - \frac{5}{3} (1 - P)^3 P - 7 (1 - P)^2 P^2 - \frac{17}{3} (1 - P) P^3 - P^4 \tag{2a}$$

$$\frac{\Gamma_{\mathrm{fatigue}}^{\mathrm{ref}} (p)}{\Gamma_{\mathrm{fatigue}}^{\mathrm{ref}} (p = 1)} = 1 - \frac{3}{4} (1 - P)^3 P - \frac{9}{2} (1 - P)^2 P^2 - \frac{19}{4} (1 - P) P^3 - P^4 \tag{2b}$$

$$P = pP^3 + 1 - p \tag{2c}$$

where $\mu^{\mathrm{ref}} (p)$ and $\Gamma_{\mathrm{fatigue}}^{\mathrm{ref}} (p)$ are the shear modulus and fatigue threshold of a polymer network with reactions efficiency p at the as-prepared reference state respectively, P is the probability of connecting to a dangling end for one arm of the macromer. In addition, the shear modulus and fatigue threshold of the ideal polymer network measured at the swollen state (*i.e.*, $\mu (p)$, $\Gamma_{\mathrm{fatigue}} (p)$) can be related to the values at the reference state (*i.e.*, $\mu^{\mathrm{ref}} (p)$, $\Gamma_{\mathrm{fatigue}}^{\mathrm{ref}} (p)$) with

$$\mu^{\mathrm{ref}} (p) = \mu (p) \lambda_s \tag{3a}$$

$$\Gamma_{\mathrm{fatigue}}^{\mathrm{ref}} (p) = \Gamma_{\mathrm{fatigue}} (p) \lambda_s^2 \tag{3b}$$

where λ_s is the swelling ratio in length (Fig. 6b). As shown in Fig. 6d, our model captures the nonlinear reduction of polymer networks' fatigue thresholds as the reaction efficiency decreases. For polymer networks with high reaction efficiency (*i.e.*, $p > 0.8$), their fatigue thresholds are approximately the same as that of ideal polymer network without defects (around 30 J/m^2). For polymer networks with low reaction efficiency (*i.e.*, $p < 0.8$), the presence of substantial dangling-chain defects dramatically decreases their fatigue thresholds.

This nonlinear trend is possibly due to the two competing mechanisms explained by our model: (i) network toughening by increasing the effective chain length, and (ii) network weakening by introducing inactive polymer chains. When the reaction efficiency is high, these two mechanisms are competing with each other, resulting in an approximately constant fatigue threshold; as the reaction efficiency further decreases, the network weakening dominates, giving a significant reduction of fatigue thresholds. By fitting the experimental data with our model, we can further identify the dimensionless parameter α as 2.4, which is approximately consistent with the theoretical value in our model (*i.e.*,
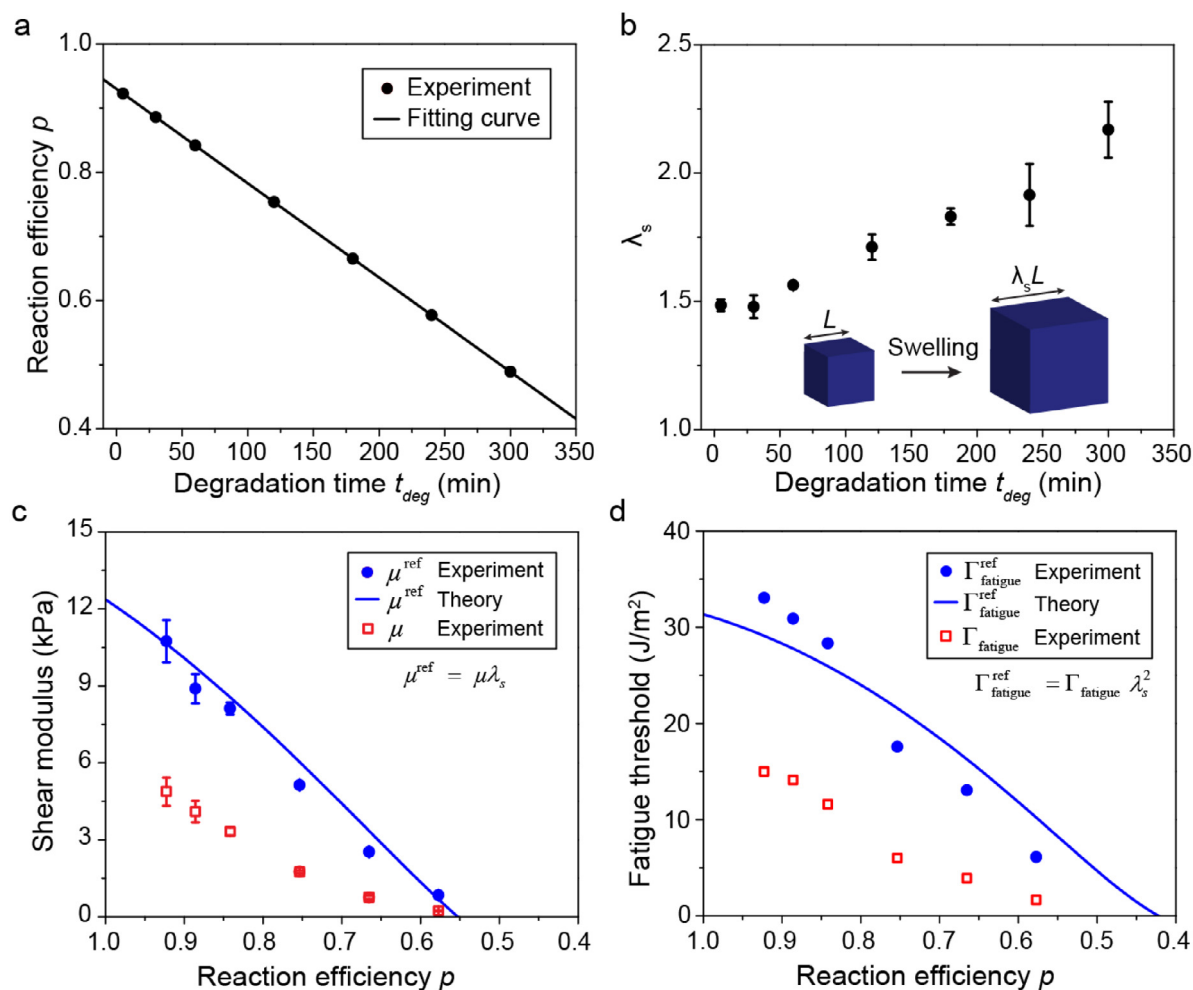
Fig. 6. Comparisons between experiment and theory. (a) Calibrated reaction efficiency p as a function of degradation time t_{deg}. (b) Measured swelling ratio in length λ_s as a function of degradation time t_{deg}. (c) The comparison of the shear modulus between experiment and theory. The hollow dots and the solid dots denote the measured shear modulus at the swollen state μ and at the reference state μ^{ref} in experiment (Fig. B.1). The solid line denotes the theoretical shear modulus at the reference state μ^{ref} fitted using the defect-network elastic model. (d) The comparison of the fatigue threshold between experiment and theory. The hollow dots and the solid dots denote the measured fatigue threshold at the swollen state Γ_{fatigue} and at the reference state $\Gamma_{\text{fatigue}}^{\text{ref}}$ in experiment. The solid line denotes the theoretical fatigue threshold at the reference state $\Gamma_{\text{fatigue}}^{\text{ref}}$ using the defect-network fracture model.

$\alpha = 2$) [26]. The quantitative agreement between the experiment and our model suggests that the A–B type tetra-arm PEG polymer network can serve as a standard material platform for polymer mechanics.

4. Conclusion

In this paper, we study the fracture and fatigue of ideal polymer networks with uniform chain length and functionality, and controlled densities of dangling-chain defects. Our experimental results ascertain that the fracture toughness and fatigue threshold of an ideal polymer network almost free of defects are the same (i.e., $\Gamma_{\text{fracture}} = \Gamma_{\text{fatigue}}$). After introducing various densities of dangling-chain defects into the ideal polymer network, its fracture toughness and fatigue threshold still maintain approximately the same. We show that the measured fracture toughness of ideal polymer networks almost without defects and with defects is independent of the loading rate. We further use the defect-network fracture model to theoretically explain the fatigue thresholds of ideal polymer networks with controlled densities of dangling-chain defects. This work shows the power of using well-designed synthetic materials as an experimental platform to facilitate fundamental studies in polymer mechanics.

CRediT authorship contribution statement

Shaoting Lin: Conceived the idea, Designed the study, Synthesized the samples, Conducted the fracture and fatigue tests, Analyzed and processed the data, Drafted the paper with comments. **Jiahua Ni:** Conducted the fracture and fatigue tests. **Dongchang Zheng:** Conducted the fracture and fatigue tests. **Xuanhe Zhao:** Conceived the idea, Designed the study, Supervision.

Declaration of competing interest

The authors declare that they have no known competing financial interests or personal relationships that could have appeared to influence the work reported in this paper.

Acknowledgments

Appendix A. Defect-network fracture model

The model focuses on a tetra-arm ideal polymer network containing only dangling chains in the form of various orders (e.g., 1st-order, 2nd-order, 3rd-order, and 4th-order). We denote the probability of connecting to a dangling end for one arm of the macromer as P. We further denote the probability of the arm to form a cross-link with one arm of the neighboring macromer as p, the probability of the arm to connect with an inactive dangling chain as $1 - p$. If the arm forms a cross-link with one arm of the neighboring macromer, the only possibility for the arm to connect with an inactive dangling chain is that all the remaining three arms of the neighboring macromer must connect to a dangling end, giving the possibility of P^3. Given this probabilistic analysis, we can write the relation between P and p as

$$P = pP^3 + 1 - p \tag{A.1}$$

Let C_X and C_{ideal} be the ratios of the numbers of defective macromers X and defect-free macromers over the total number of macromers that constitute the polymer network, respectively. The number conservation of macromers imposes

$$\sum_X C_X + C_{\text{ideal}} = 1 \tag{A.2}$$

Specifically, the possibility of defect-free macromers among the overall macromers is $C_{\text{ideal}} = (1 - P)^4$ since all arms of the macromers remain active. The possibility of defective macromers with 1st-order dangling chain among the overall macromers is $C_{1d} = 4(1 - P)^3 P$, since one arm of the defective macromer is inactive while the other three remain active. Likewise, we can calculate the possibility of defective macromers with 2nd-order dangling chain, 3rd-order dangling chain, 4th-order dangling chain as $C_{2d} = 6(1 - P)^2 P^2$, $C_{3d} = 4(1 - P)P^3$, $C_{4d} = P^4$, respectively. Once the macromers are crosslinked, they form a polymer network containing different types of active polymer chains. We regard the chain as an affected polymer chain due to the defect X if the active polymer chain is the closest chain to a defect X; otherwise, we regard the active polymer chain as an unaffected polymer chain. The number of affected chains due to a defect X is denoted as N_X^{affected}, the number of unaffected chains is denoted as $N^{\text{unaffected}}$, and the total number of polymer chains in the corresponding defect-free ideal polymer network is denoted as N^{total}. Since one defective macromer (except 4th-order dangling chain) affects one polymer chain on the crack path and one chain is shared by two macromers, the number of affected chains due to a defect X is $N_X^{\text{affected}} = 0.5C_X N^{\text{total}}$. In addition to the active polymer chains, defects X also introduce inactive polymer chains with the number of N_X^{inactive}. The number conservation of chains imposes

$$\sum_X \left(N_X^{\text{affected}} + N_X^{\text{inactive}} \right) + N^{\text{unaffected}} = N^{\text{total}} \tag{A.3}$$

The presence of one 1st-order dangling chain introduces 0.25 inactive chains since one-fourth of the arms of the defective macromer is inactive, i.e., $N_{1d}^{\text{inactive}} = 0.25C_{1d}N^{\text{total}}$ (Fig. A.1b). The presence of one 2nd-order dangling chain only increases the length of an originally existing chain, thereby all the arms are equivalently inactive, giving the number of inactive chains as $N_{2d}^{\text{inactive}} = C_{2d}N^{\text{total}}$ (Fig. A.1b). All the arms of one defective macromer with a 3rd-order dangling chain are elastically inactive. In addition, the presence of one 3rd-order dangling chain produces one additional inactive arm of the neighboring macromer, thereby giving the total number of inactive chains as $N_{3d}^{\text{inactive}} = 1.25C_{3d}N^{\text{total}}$ (Fig. A.1b). The defective macromer with 4th-order

dangling chain is a leaving macromer with no topological connection with the polymer network, thereby giving the number of inactive chains as $N_{4d}^{\text{inactive}} = C_{4d}N^{\text{total}}$. Following Eq. (A.3), we can calculate the total number of inactive chains due to the defects as

$$\sum_X N_X^{\text{inactive}} = (0.25C_{1d} + C_{2d} + 1.25C_{3d} + C_{4d})N^{\text{total}} \tag{A.4}$$

It should be noted that the above calculation of the number of inactive chains is overestimated when the ideal polymer network contains high-density defects since the above calculation neglects the coupling between defective macromers. Here, we also provide the calculation of the lower bound for the number of inactive chains of ideal polymer networks with various reaction efficiency p. We start with the calculation of the total number of active chains. Only defective macromers with 1st-order dangling chain and defective-free macromers produce active polymer chains. The presence of one defective macromer with 1st-order dangling chain produces 0.75 active chains in total, while the presence of one defect-free macromer produces one active chains in total. The total number of active chains in an ideal polymer network is equal to $(0.75C_{1d} + C_{\text{ideal}})N^{\text{total}}$, namely,

$$\sum_X N_X^{\text{affected}} + N^{\text{unaffected}} = \left(\frac{3}{4}C_{1d} + C_{\text{ideal}} \right)N^{\text{total}} \tag{A.5}$$

Equivalently, the total number of inactive chains in an ideal polymer network containing dangling-chain defects is equal to

$$\sum_X N_X^{\text{inactive}} = \left(1 - \frac{3}{4}C_{1d} - C_{\text{ideal}} \right)N^{\text{total}} \tag{A.6}$$

where $C_{1d} = 4(1 - P)^3 P$ and $C_{\text{ideal}} = (1 - P)^4$. Fig. A.2a plots the upper bound and lower bound of the number of inactive chains in an ideal polymer network with various reaction efficiency p using Eq. (A.4) and Eq. (A.6), respectively. Notably, the two calculations give consistent results when the introduced density of defects is low, where the coupling effects between defects are negligible.

Once a crack propagates in an ideal polymer network, it fractures unaffected chains as well as affected chains by different types of defects (Fig. A.1a). We denote the effective energy relaxed by fracturing an unaffected polymer chain in an ideal polymer network as U_{ideal} and the effective energy relaxed by fracturing an affected polymer chain by a defect X as U_X. The ratio of U_X over U_{ideal} defines the fracture effectiveness of an active polymer chain as $\gamma_X = U_X/U_{\text{ideal}}$, which characterizes the energy contribution of an active polymer chain to the intrinsic fracture energy of an ideal polymer network compared with that of an unaffected polymer chain in the polymer network. Following our recent work [26], the fracture effectivenesses of an affected polymer chain, a 1st-order dangling chain, a 2nd-order dangling chain, a 3rd-order dangling chain are equal to 1, 9/8, 3/2, and 9/8, respectively (Fig. A.1b). Overall, the intrinsic fracture energy of the polymer network with defects normalized by that of the corresponding defect-free ideal network can be expressed as

$$\overline{\Gamma} = \sum_X \gamma_X \frac{N_X^{\text{affected}}}{N^{\text{total}}} + \frac{N^{\text{unaffected}}}{N^{\text{total}}} \tag{A.7}$$

Alternatively, the normalized intrinsic fracture energy of polymer networks can be expressed as

$$\overline{\Gamma} = \sum_X (\gamma_X - 1) \frac{N_X^{\text{affected}}}{N^{\text{total}}} - \sum_X \frac{N_X^{\text{inactive}}}{N^{\text{total}}} + 1 \tag{A.8}$$

where the first term $\sum_X (\gamma_X - 1) N_X^{\text{affected}}/N^{\text{total}}$ characterizes the toughening effect due to the increased chain length since $\gamma_X \geq 1$
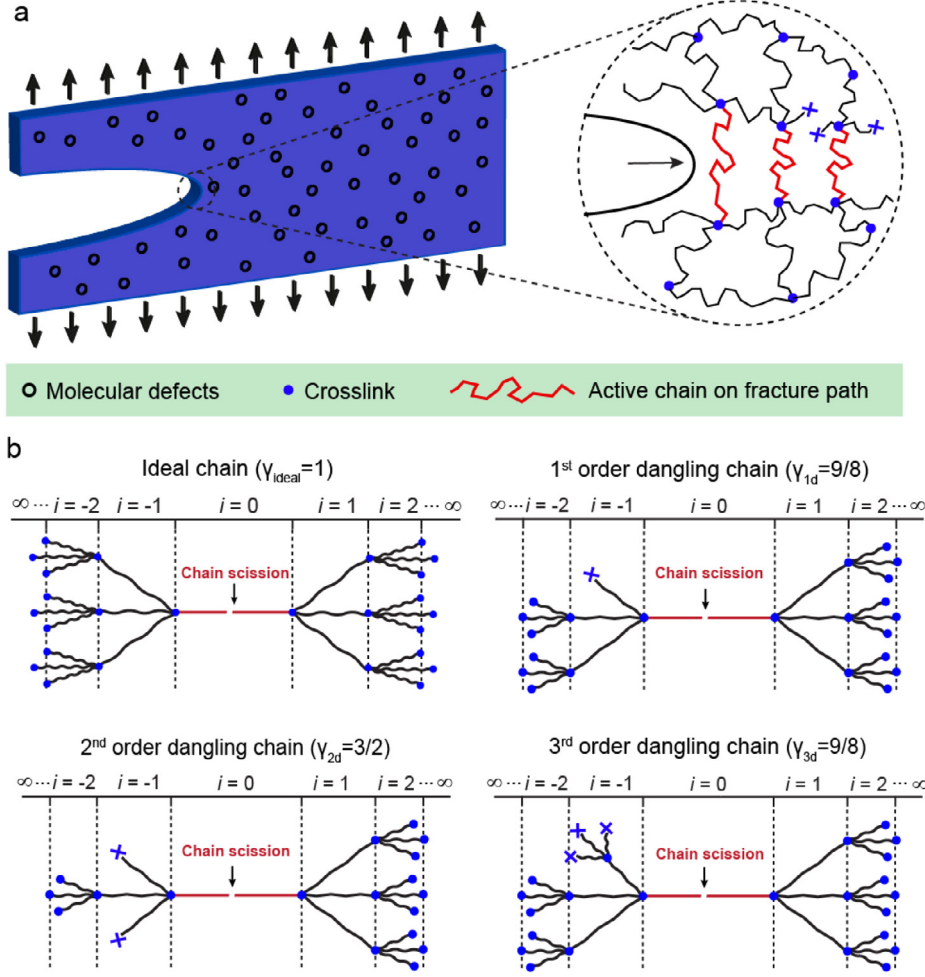
Fig. A.1. Illustration of defect-network fracture model. (a) Schematic illustration of the key concept for the defect-network fracture model: crack propagates by fracturing unaffected polymer chains as well as affected chains due to defects. (b) Schematic illustration of a fractured polymer chain on the crack path and deformed neighboring chains. Depending on the type of the fractured polymer chain, it gives different fracture effectiveness. The fracture effectiveness of an ideal polymer chain and the most affected chain by 1st-order dangling chain, 2nd-order dangling chain, and 3rd-order dangling chain is 1, 9/8, 3/2, and 9/8, respectively. Panels (a) and (b) are reproduced with permission from ref. [26].
© 2020 by the American Physical Society.

and the second term $\sum_X N_X^{\text{inactive}}/N^{\text{total}}$ characterizes the weakening effect due to the reduced active chain density.

Given the identified fracture effectiveness of active polymer chains γ_X, the number of inactive chains N_X^{inactive} and the number of affected chains N_X^{affected} due to the presence of defect X, we can write the normalized intrinsic fracture energy of ideal polymer networks as a function of the reaction efficiency p,

$$\overline{\Gamma} = \frac{\Gamma(p)}{\Gamma(p=1)} = 1 - \frac{3}{4}(1-P)^3 P - \frac{9}{2}(1-P)^2 P^2$$
$$- \frac{19}{4}(1-P)P^3 - P^4 \tag{A.9}$$

where $P = pP^3 + 1 - p$, $\Gamma(p)$ is the intrinsic fracture energy of an ideal polymer network with reaction efficiency p, $\Gamma(p=1)$ is the intrinsic fracture energy of an ideal polymer network with no defects. Alternatively, using Eq. (A.6) as the number of total inactive chains in an ideal polymer network and given the number of affected chains by defect X equal to $N_X^{\text{affected}} = 0.5C_X N^{\text{total}}$, we can also calculate the normalized intrinsic fracture energy of ideal polymer networks as

$$\overline{\Gamma} = \frac{\Gamma(p)}{\Gamma(p=1)} = (1-P)^4 + \frac{13}{4}(1-P)^3 P$$

$$+ \frac{3}{2}(1-P)^2 P^2 + \frac{1}{4}(1-P)P^3 \tag{A.10}$$

where $P = pP^3 + 1 - p$. Fig. A.2b plots the comparison of the calculated normalized intrinsic fracture energy using Eq. (A.9) and Eq. (A.10), respectively.

Appendix B. Defect-network elastic model

For a tetra-arm ideal polymer network, given its reaction efficiency p, the number densities of defect-free macromer and various orders of defective macromers are equal to $C_{\text{ideal}} = (1-P)^4$, $C_{1d} = 4(1-P)^3 P$, $C_{2d} = 6(1-P)^2 P^2$, $C_{3d} = 4(1-P)P^3$, and $C_{4d} = P^4$, where $P = pP^3 + 1 - p$. Once the macromers are crosslinked, they form a polymer network containing different types of active polymer chains: unaffected polymer chains with the number of $N^{\text{unaffected}}$ and affected polymer chains due to defects X with the number of N_X^{affected}. In addition to the active polymer chains, defects X also introduce inactive polymer chains with the number of N_X^{inactive}. The number conservation of chains imposes $\sum_X \left(N_X^{\text{affected}} + N_X^{\text{inactive}}\right) + N^{\text{unaffected}} = N^{\text{total}}$ where N^{total} is the total number of polymer chains in the corresponding defect-free ideal network. The number of inactive chains in defect-network elastic model is the same as that in defect-network fracture model. However, the numbers of affected chains
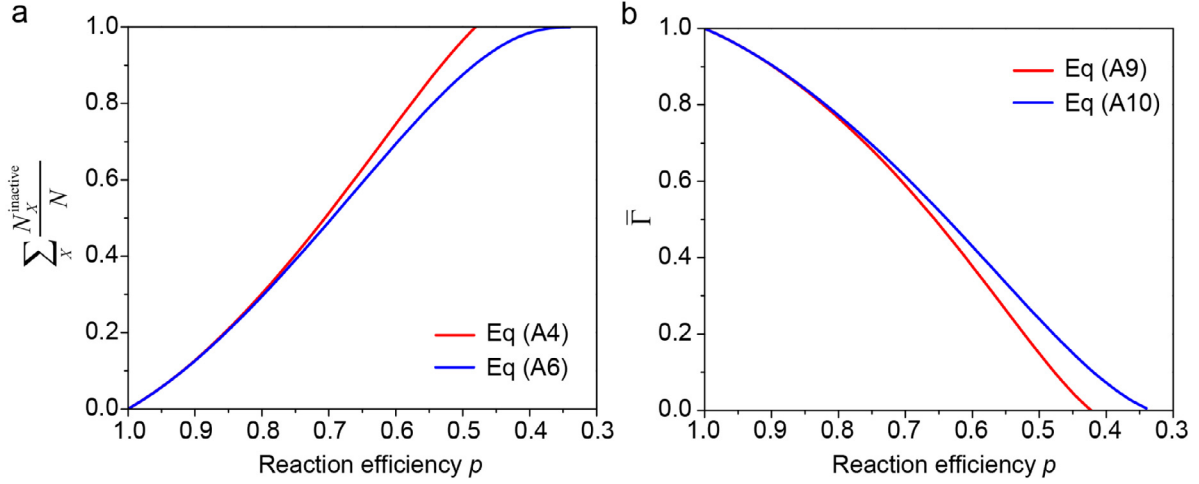
Fig. A.2. (a) Calculations of the upper bound and lower bound of the total number of inactive chains as a function of reaction efficiency p using Eq. (A.4) and Eq. (A.6), respectively. (b) Calculations of the lower bound and upper bound of the normalized intrinsic fracture energy as a function of reaction efficiency p using Eq. (A.9) and Eq. (A.10), respectively.
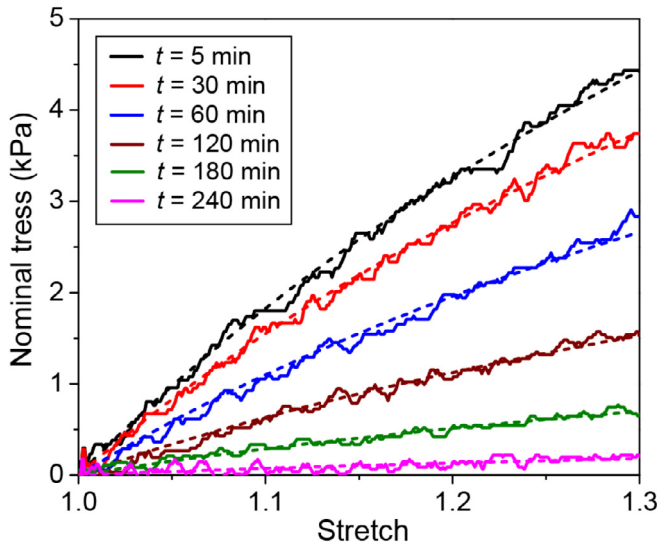
Fig. B.1. Determination of shear moduli of ideal polymer networks. The measured shear modulus is extracted by fitting the nominal stress versus stretch curve ranging from $\lambda = 1$ to $\lambda = 1.3$ using $S = \mu (\lambda - \lambda^{-3})$, where S is the nominal stress, λ is stretch, and μ is shear modulus. Solid lines are experimentally measured curves, and dashed lines are fitted curves using $S = \mu (\lambda - \lambda^{-3})$.

and unaffected chains due to the presence of defect X are different between the two models since one defective macromer affects multiple active chains in defect-network elastic model while one defective macromer affects only one chain in defect-network fracture model. Specifically, the number of affected chains due to the presence of a 1st-order defective macromer is $N_{1d}^{\text{affected}} = 1.5C_{1d}N^{\text{total}}$ since one defective macromer affects three polymer chains equivalently and one active chain is equally shared by two macromers. Similarly, the number of affected chains due to the presence of a 3rd-order defective macromer is $N_{3d}^{\text{affected}} = 1.5C_{3d}N^{\text{total}}$. The number of affected chains due to the presence of a 2nd-order defective macromer is $N_{2d}^{\text{affected}} = 0.5C_{2d}N^{\text{total}}$ since one defective macromer affects two polymer chains equivalently and one active chain is shared by two macromers. The presence of 4th-order defective macromer introduces no affected chains, namely, $N_{4d}^{\text{affected}} = 0$.

We denote the effective chain length by elastically deforming an unaffected polymer chain in an ideal polymer network as M_{ideal} and the effective chain length by elastically deforming an affected polymer chain by a defect X as M_X. The ratio of M_{ideal} over M_X defines the elastic effectiveness of an active polymer chain as $\varepsilon_X = M_X/M_{\text{ideal}}$, which characterizes the entropic energy contribution of an active polymer chain to the elastic shear modulus of the corresponding polymer network compared with that of an unaffected polymer chain in an ideal polymer network. The elastic effectiveness of 1st-order dangling chain, 2nd-order dangling chain, 3rd-order dangling chain, 4th-order dangling chain is equal to 8/9, 2/3, 8/9, and 0, respectively [26]. Overall, the shear modulus of the polymer network with defects normalized by that of the corresponding defect-free ideal network can be expressed as

$$\overline{\mu} = \sum_X \varepsilon_X \frac{N_X^{\text{affected}}}{N^{\text{total}}} + \frac{N^{\text{unaffected}}}{N^{\text{total}}} \tag{B.1}$$

Alternatively, the shear modulus of polymer networks can be expressed as

$$\overline{\mu} = \sum_X (\varepsilon_X - 1) \frac{N_X^{\text{affected}}}{N^{\text{total}}} - \sum_X \frac{N_X^{\text{inactive}}}{N^{\text{total}}} + 1 \tag{B.2}$$

The first term in Eq. (B.2) characterizes the reduction of shear modulus due to the increased chain length by defects, and the second term characterizes the reduction of shear modulus due to the presence of inactive chains.

Given the identified elastic effectiveness of active polymer chains ε_X, number of inactive chains N_X^{inactive} and number of affected chains N_X^{affected} due to the presence of defect X, we can write the normalized shear modulus of ideal polymer network as a function of the reaction efficiency p,

$$\overline{\mu} = \frac{\mu (p)}{\mu (p = 1)} = 1 - \frac{5}{3} (1 - P)^3 P - 7 (1 - P)^2 P^2 - \frac{17}{3} (1 - P) P^3 - P^4 \tag{B.3}$$

where $P = pP^3 + 1 - p$, $\mu (p)$ is the shear modulus of the ideal polymer network with reaction efficiency of p, and $\mu (p = 1) = 0.5NkT$ is the shear modulus of the ideal polymer network without defects predicted by the phantom network model [49,50].

References

[1] Y. Kim, G.A. Parada, S. Liu, X. Zhao, Sci. Robot. 4 (2019).

[2] T. Li, G. Li, Y. Liang, T. Cheng, J. Dai, X. Yang, B. Liu, Z. Zeng, Z. Huang, Y. Luo, Sci. Adv. 3 (2017) e1602045.

[3] G. Mao, M. Drack, M. Karami-Mosammam, D. Wirthl, T. Stockinger, R. Schwödiauer, M. Kaltenbrunner, Sci. Adv. 6 (2020) eabc0251.

[4] H. Yuk, B. Lu, S. Lin, K. Qu, J. Xu, J. Luo, X. Zhao, Nat. Com. 11 (2020) 1.

[5] H. Yuk, B. Lu, X. Zhao, Chem. Soc. Rev. 48 (2019) 1642.

[6] S. Lin, H. Yuk, T. Zhang, G.A. Parada, H. Koo, C. Yu, X. Zhao, Adv. Mater. 28 (2016) 4497.

[7] J. Deng, H. Yuk, J. Wu, C.E. Varela, X. Chen, E.T. Roche, C.F. Guo, X. Zhao, Nature Mater. 1 (2020).

[8] H. Yuk, C.E. Varela, C.S. Nabzdyk, X. Mao, R.F. Padera, E.T. Roche, X. Zhao, Nature 575 (2019) 169.

[9] J. Li, A. Celiz, J. Yang, Q. Yang, I. Wamala, W. Whyte, B. Seo, N. Vasilyev, J. Vlassak, Z. Suo, Science 357 (2017) 378.

[10] X. Liu, H. Yuk, S. Lin, G.A. Parada, T.C. Tang, E. Tham, C. de la Fuente-Nunez, T.K. Lu, X. Zhao, Adv. Mater. 30 (2018) 1704821.

[11] J. Guo, X. Liu, N. Jiang, A.K. Yetisen, H. Yuk, C. Yang, A. Khademhosseini, X. Zhao, S.H. Yun, Adv. Mater. 28 (2016) 10244.

[12] X. Liu, T.-C. Tang, E. Tham, H. Yuk, S. Lin, T.K. Lu, X. Zhao, Proc. Natl. Acad. Sci. USA 114 (2017) 2200.

[13] F. Zhao, X. Zhou, Y. Shi, X. Qian, M. Alexander, X. Zhao, S. Mendez, R. Yang, L. Qu, G. Yu, Nat. Nanotechnol. 13 (2018) 489.

[14] Y. Guo, X. Zhao, F. Zhao, Z. Jiao, X. Zhou, G. Yu, Energy Environ. Sci. 13 (2020) 2087.

[15] F. Zhao, Y. Guo, X. Zhou, W. Shi, G. Yu, Nat. Rev. Mater. 5 (2020) 388.

[16] R. Long, C.-Y. Hui, Soft Matter 12 (2016) 8069.

[17] T. Zhang, S. Lin, H. Yuk, X. Zhao, Extreme Mech. Lett. 4 (2015) 1.

[18] S. Suresh, Fatigue of Materials, Cambridge University Press, 1998.

[19] R. Bai, J. Yang, Z. Suo, Eur. J. Mech. A Solids 74 (2019) 337.

[20] G. Lake, A. Thomas, Proc. R. Soc. Lond. Ser. A Math. Phys. Eng. Sci. 300 (1967) 108.

[21] K. Shimokawa, K. Ishihara, Y. Tezuka, Topology of Polymers, Springer, 2019.

[22] Y. Gu, J. Zhao, J.A. Johnson, Trends Chem. 1 (2019) 318.

[23] C. Yang, T. Yin, Z. Suo, J. Mech. Phys. Solids 131 (2019) 43.

[24] J. Slootman, V. Waltz, C.J. Yeh, C. Baumann, R. Göstl, J. Comtet, C. Creton, Phys. Rev. X 10 (2020) 041045.

[25] T. Matsuda, R. Kawakami, T. Nakajima, J.P. Gong, Macromolecules 53 (2020) 8787.

[26] S. Lin, X. Zhao, Phys. Rev. E 102 (2020) 052503.

[27] Y. Akagi, H. Sakurai, J.P. Gong, U.-i. Chung, T. Sakai, J. Chem. Phys. 139 (2013) 144905.

[28] T. Matsunaga, T. Sakai, Y. Akagi, U.-i. Chung, M. Shibayama, Macromolecules 42 (2009) 1344.

[29] T. Sakai, T. Matsunaga, Y. Yamamoto, C. Ito, R. Yoshida, S. Suzuki, N. Sasaki, M. Shibayama, U.-i. Chung, Macromolecules 41 (2008) 5379.

[30] M. Shibayama, X. Li, T. Sakai, Colloid Polym. Sci. 297 (2019) 1.

[31] T. Hiroi, M. Ohl, T. Sakai, M. Shibayama, Macromolecules 47 (2014) 763.

[32] Y. Akagi, T. Katashima, Y. Katsumoto, K. Fujii, T. Matsunaga, U.-i. Chung, M. Shibayama, T. Sakai, Macromolecules 44 (2011) 5817.

[33] M. Zhong, R. Wang, K. Kawamoto, B.D. Olsen, J.A. Johnson, Science 353 (2016) 1264.

[34] T.-S. Lin, R. Wang, J.A. Johnson, B.D. Olsen, Macromolecules 51 (2018) 1224.

[35] R. Bai, Q. Yang, J. Tang, X.P. Morelle, J. Vlassak, Z. Suo, Extreme Mech. Lett. 15 (2017) 91.

[36] G. Lake, P. Lindley, J. Appl. Polym. Sci. 9 (1965) 1233.

[37] W. Fan, Y. Wang, S. Cai, Polym. Test. 61 (2017) 373.

[38] W. Zhang, X. Liu, J. Wang, J. Tang, J. Hu, T. Lu, Z. Suo, Eng. Fract. Mech. 187 (2018) 74.

[39] X. Li, K. Cui, T.L. Sun, L. Meng, C. Yu, L. Li, C. Creton, T. Kurokawa, J.P. Gong, Proc. Natl. Acad. Sci. USA 117 (2020) 7606.

[40] S. Lin, X. Liu, J. Liu, H. Yuk, H.-C. Loh, G.A. Parada, C. Settens, J. Song, A. Masic, G.H. McKinley, Sci. Adv. 5 (2019) eaau8528.

[41] S. Lin, J. Liu, X. Liu, X. Zhao, Proc. Natl. Acad. Sci. USA 116 (2019) 10244.

[42] E. Zhang, R. Bai, X.P. Morelle, Z. Suo, Soft Matter 14 (2018) 3563.

[43] J. Tang, J. Li, J.J. Vlassak, Z. Suo, Extreme Mech. Lett. 10 (2017) 24.

[44] H. Watanabe, Prog. Polym. Sci. 24 (1999) 1253.

[45] B. Persson, E. Brener, Phys. Rev. E 71 (2005) 036123.

[46] R. Long, K. Mayumi, C. Creton, T. Narita, C.-Y. Hui, Macromolecules 47 (2014) 7243.

[47] T.L. Sun, T. Kurokawa, S. Kuroda, A.B. Ihsan, T. Akasaki, K. Sato, M.A. Haque, T. Nakajima, J.P. Gong, Nature Mater. 12 (2013) 932.

[48] Y. Mao, S. Lin, X. Zhao, L. Anand, J. Mech. Phys. Solids 100 (2017) 103.

[49] M. Rubinstein, R.H. Colby, Polymer Physics, vol. 23, Oxford University Press, New York, 2003.

[50] P. Flory, J. Chem. Phys. 66 (1977) 5720.

[51] M. Grandbois, M. Beyer, M. Rief, H. Clausen-Schaumann, H.E. Gaub, Science 283 (1999) 1727.

[52] J. Cui, M.A. Lackey, G.N. Tew, A.J. Crosby, Macromolecules 45 (2012) 6104.

[53] S. Wang, S. Panyukov, M. Rubinstein, S.L. Craig, Macromolecules 52 (2019) 2772.

[54] Y. Mao, B. Talamini, L. Anand, Extreme Mech. Lett. 13 (2017) 17.

[55] A. Arora, T.-S. Lin, H.K. Beech, H. Mochigase, R. Wang, B.D. Olsen, Macromolecules 53 (2020) 7346.